*sustainability*

MDPI

*Article*

# Experimental and Numerical Analysis on Effect of Passive Cooling Methods on an Indoor Thermal Environment Having Floor-Level Windows

**Beilei Qin [1], Xi Xu [2,*], Takashi Asawa [3] and Lulu Zhang [4]**

[1] Dassault Systèmes K.K, ThinkPark Tower, 2-1-1 Osaki, Shinagawa-ku, Tokyo 141-6020, Japan; beilei.qin@3ds.com
[2] School of Spatial Planning and Design, Zhejiang University City College, Hangzhou 310015, China
[3] Department of Architecture and Building Engineering, Tokyo Institute of Technology, 4259 Nagatsuta-cho, Midroi-ku, Yokohama 226-8502, Japan; asawa.t.aa@m.titech.ac.jp
[4] College of Civil Engineering and Architecture, Tongji University, 1239 SiPing Rd, Shanghai 200092, China; zhang_lulu@tongji.edu.cn
* Correspondence: xuxi@zucc.edu.cn; Tel.: +81-459245510; Fax: +81-459245553

**Abstract:** Natural ventilation is a common passive cooling method for improving air quality and thermal comfort; however, hot temperatures in summer and safety and privacy issues at night often result in its unideal performance. Therefore, we proposed the use of floor-level windows, mainly combined with microclimate improvement, to improve the indoor thermal environment by enhancing the cooling effect of natural ventilation during summer. Our study area was a house in Machida, Tokyo. We evaluated the effectiveness of our method in improving the indoor thermal environment in summer and performed a numerical simulation, while illustrating the detailed horizontal and vertical distribution of airflow in the house through the floor-level windows. The influence of different window types and opening angles of floor-level windows on ventilation and cooling was determined using the simulation. We found that: (a) natural ventilation-based passive cooling methods reduced semi-outdoor and indoor temperature and increased the humidity; (b) the airflow formed an indoor wind path; south-westerly inflow was from western floor-level windows and the skylight, and the outflow was from northern floor-level windows; and (c) the side hung windows (with an opening angle of 60°) were an ideal option to improve indoor airflow. However, there was no improvement in the passive cooling performance, due to the inflow of warmer outside air.

**Keywords:** passive cooling method; natural ventilation; floor-level windows; microclimate improvement; numerical analysis; indoor air quality; side hung type

check for updates

**Citation:** Qin, B.; Xu, X.; Asawa, T.; Zhang, L. Experimental and Numerical Analysis on Effect of Passive Cooling Methods on an Indoor Thermal Environment Having Floor-Level Windows. *Sustainability* **2022**, *14*, 7880. https://doi.org/10.3390/su14137880

Academic Editor: Francesco Contò

Received: 25 April 2022
Accepted: 21 June 2022
Published: 28 June 2022

**Publisher's Note:** MDPI stays neutral with regard to jurisdictional claims in published maps and institutional affiliations.

**Copyright:** © 2022 by the authors. Licensee MDPI, Basel, Switzerland. This article is an open access article distributed under the terms and conditions of the Creative Commons Attribution (CC BY) license (https://creativecommons.org/licenses/by/4.0/).

## 1. Introduction

Global warming has been observed and studied by scientists at NASA's Goddard Institute for Space Studies (GISS) since 1880; the average global temperature on Earth has increased by more than 1 °C [1], which has increased the need for more efficient cooling methods in summer. With the development of economies and rapid urbanization, thermal environments have been controlled using artificial means, such as fans, air conditioners and coolers [2]. The International Energy Agency (IEA) reports that almost 20% of the total electricity used in buildings around the world today is consumed to maintain cool temperatures by using air conditioners and electric fans [3]. Although the demand for cooling can be satisfied using such devices, it still brings heavy burdens to the economy and environment simultaneously, due to greenhouse gas (GHG) emissions.

Compared to the energy consumed for satisfying cooling demands using fans and air conditioners, passive cooling methods are simple and lower the indoor air temperatures of buildings naturally [4], with limited or no energy-consuming mechanical equipment [5]; thus, they are more economical and environment-friendly [6]. As one of the main passive

cooling methods, natural ventilation is widely used in the passive design of buildings because it can improve the indoor thermal environment and comfort, as well as reduce energy consumption and improve air quality [7]. Moreover, the acceptable thermal comfort range is even larger in ventilated buildings than in buildings equipped with heating, ventilation, and air-conditioning systems [8]. Overall, it is common to introduce outdoor air into interior space directly, and this process is called direct ventilation. Direct ventilation mostly depends on the difference between indoor and outdoor temperature and the airflow rate, which is also limited by the thermal mass and cooling demand of a target building [9]. Consequently, natural ventilation is not always as efficient as it should be, especially when the local weather condition is not pleasant. Natural ventilation when the outside air is warmer can lead to a negative impact on the indoor thermal environment unless improvement measures are implemented.

To utilize natural ventilation during daytime in summer, the outdoor air to be introduced must be cooler than the indoors. To address this issue, improvements in microclimate, as another effective passive cooling method, is considered a feasible measure. Microclimate is defined as the climate of one specified area, which is generally different from regional or global climate patterns [10]. Apart from its correlation with local climate, it can be influenced by plants [11], human activities [12], and water resources [13]. Studies have proved that passive cooling strategies, especially a combination of multiple passive cooling methods, such as evaporative cooling materials, vegetation, and dripping water, are effective methods to improve the microclimate; thus, they comprise common elements in the passive cooling design process for a normal building [14,15]. However, nighttime ventilation is more often used in summer because outdoor temperature at night is much lower than that in daytime, which reduces the thermal demand by applying the heat absorbed in daytime [16]. Some studies increased the cooling effect of night ventilation by improving the microclimate, which can be regarded as a typically effective combination of passive cooling methods. For example, Toe et al. [17] investigated and confirmed the cooling effects of small courtyards on structures with high thermal mass through nocturnal ventilative (opening of all windows of the whole study house) and radiative cooling. Additionally, Xie et al. [18] proved that the microclimate caused by the courtyard form (a typical type of built form) enhanced the cooling effect of night ventilation. However, extensive night ventilation poses safety and privacy problems through window openings, and this situation could be even more concerning for low-rise detached houses in urban areas. This issue has not been considered in the abovementioned studies conducted on the cooling performance of combined passive cooling methods.

For ventilation and better living environments, lattice-doors/windows, high windows, floor-level windows, and flying corridors are the most commonly used methods [19]. Floor-level windows are generally adjacent to the floor or in the lower part of the wall and generally have a smaller size than normal windows; thereby, satisfying the ventilation and safety demand simultaneously. They are common in traditional Japanese architecture, particularly in tea houses [20,21]. In snowy regions, light from the ground can be introduced inside by floor-level windows [22]. Additionally, floor-level windows can be combined with phase change material for cold storage during night ventilation [23] and green roofs for thermal performance [24].

Thus, owing to non-ideal meteorological conditions in summer daytime and safety and privacy issues associated with extended ventilation during nighttime, natural ventilation through floor-level windows, combined with other passive cooling methods, can improve the indoor microclimate on summer days. In this study, we selected a house in Machida, a city in Tokyo, to investigate the effectiveness of the proposed cooling methods in improving the indoor thermal environment in summer. The results are shown and discussed in terms of the spatial distribution of air temperature and relative humidity. Notably, we also performed a well-validated simulation to illustrate the detailed horizontal and vertical distribution of airflow in the house. Furthermore, the influence of different window types and opening angles of floor-level windows on the ventilation and cooling performance

of the proposed passive cooling methods was determined by numerical simulation; the quality and reliability of our method was pre-tested, based on the experiment-simulation result comparison of the study house. The simulation results are discussed in terms of the velocity and direction of wind, as well as the standard effective temperature* (SET*), which is a standardized thermal comfort index, along with an overall evaluation of the cooling effect of passive designs, while focusing on the effects of window types and opening angle on the cooling effect of the proposed passive cooling methods.

## 2. Methods

### *2.1. Study House and Its Passive Cooling Design*

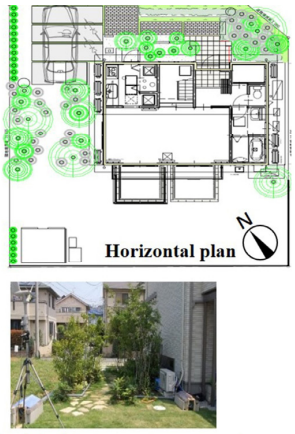
The study house was a typical two-story detached house with a wooden structure, located in Machida, Tokyo (35.58 N, 139.47 E). It faced a direction of 40° south by west. As it is mainly surrounded by low-rise residential houses, there was almost no traffic passing by.

To the south of the experiment site, there was a spacious courtyard, and a 4-m wide road was next to the courtyard. The Tsurukawa River flows approximately 20 m away from the site and there were no obstacles in the prevailing wind direction of the house. In addition to the floor-level windows, which were investigated as the main passive cooling in this study, the skylight and other normal windows were also set in the study house, to achieve the natural cross and stack ventilation of the whole house. The façade of the study house is shown in Figure 1a from different directions, showing the position of the floor-level windows and the skylight, which were important components for natural ventilation in the study house. For the exterior greening design of the site area, a horizontal plan and a photo of the current condition are shown in Figure 1b; the basic information is summarized in Figure 1c. Most plants were on the western side of the house, and primarily included shrubs, trees, and flowers; some of the shrubs were separately planted in the north.

(**a**)




(**b**)




(**c**)

| | |
|---|---|
| **Structure** | Wooden panels |
| **Average heat loss coefficient** | 2.19W/m$^2$K |
| **Site area** | 279.33 m$^2$ |
| **Total floor area** | 108.47 m$^2$ |
| **Built-up area** | 57.13 m$^2$ |

**Figure 1.** Basic information of the study house analyzed in this study: (**a**) façade of the house from four sides; (**b**) exterior layout of the house, with its horizontal plan and photo of the current condition; and (**c**) important information about the different parameters of the house.

Regarding the passive cooling methods applied in this study house, there were two floor-level windows in the western and northern walls of the first floor, of which the

opening angle was determined as 30° considering the safety problem. Detailed information about the floor-level windows is presented in Table 1. With a skylight, it was possible to determine a ventilation path; cool air entered the house through the floor-level windows and hot air escaped from the skylight because of stack-driven and wind-driven ventilation.

**Table 1.** Details of floor-level windows.

| Type | Top Hung Window (30°) |
|---|---|
| Size | 800 × 400 mm |
| Total amount | 2 in the west, 2 in the north |
| Heat transmission coefficient | 2.91 W/m$^2$·K |
| Flow coefficient ($\alpha$) | 0.7 |

Our experiment was conducted on typical summer days, and a shaded semi-outdoor space surrounding the house and in front of the western floor-level windows was selected as the target space. Plants, a water retentive block, and dripping pipes were selected as components of the passive cooling design. As shown in Figure 2, a before-and-after contrast offers a more intuitive explanation of the environmental changes in front of the western floor-level windows.

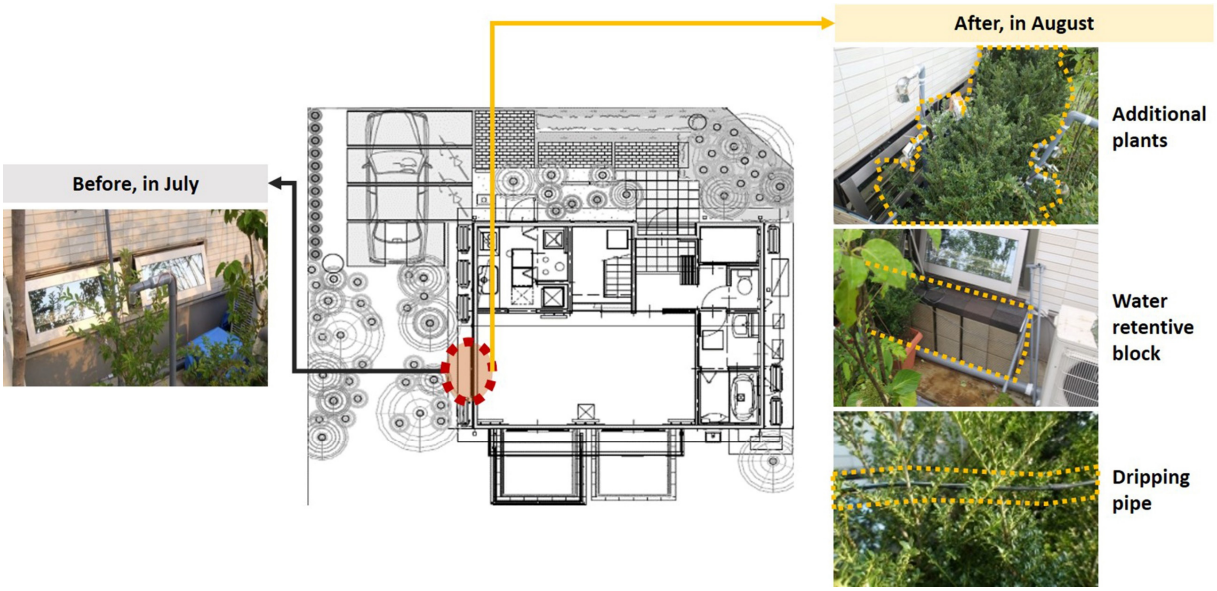



**Figure 2.** Floor-level windows before (**left**) and after (**right**) the passive cooling design.

To improve the transpiration performance of plants, we selected boxwood with small single leaves, but higher leaf density. Plants can reduce ambient temperature through evapotranspiration and wind-induced air infiltration [25,26]; boxwood encircled the semi-outdoor space in front of the floor-level windows. There was also a ceramic board in the north to prevent the cooling air from escaping. The height of the boxwood was kept higher than the top side of floor-level windows because it prevented hot air from invading the indoor space and direct solar radiation.

A water retentive block, made from a concrete block with a high water-absorbing quality, can lower the surface temperature by evaporation [27], which is a mitigation measure for the outdoor thermal environment [28]. It was placed under the floor-level windows, and its top was about 0.07 m lower than the bottom of the windows. The block volume was approximately 1.7 m × 0.3 m × 0.5 m.

Water sprinkling is another mitigation method used to improve the thermal environment [29]. In addition to their evaporative cooling effect, the dripping pipes play an important role in irrigating plants and supplying water to the water retentive block. There

were two dripping pipes; one placed among the boxwood at the height of ground level (GL) + 1 m, and the other placed on the surface of the water retentive block next to the western exterior wall.

### *2.2. Experiment*

The experiment was conducted to figure out whether the passive cooling design could contribute to reducing air temperature, and the measured data (indoor temperature, wind velocity, etc.) were also used to validate the simulated results.

#### 2.2.1. Experiment Condition

The experiment conditions for the study house are summarized in Table 2. The room was unoccupied and there was no furniture inside during the measurement period. Passive cooling items were added in front of the western floor-level windows in August so that the experiment results in July and August could be compared.

A weather station (VAISALA WXT520) was placed on the roof at the height of GL + 8.3 m, which was used to measure the air temperature, relative humidity, wind velocity and direction, and outdoor meteorological conditions on 12 July and 29 August 2014 (Figure 3).

On 12 July (Case A), all windows were kept open 24 h for ventilation, and the swinging windows were kept open from 8:30 to 18:00. The original sprinkling rate of the dripping pipes was about 0.1 L/min, continuing for 5 min at appointed times in a day. However, on 29 August (Case B), with passive cooling, the ventilation only depended on the floor-level windows on the first floor and the skylight on the roof. The sprinkling rate of the dripping pipes was changed to 0.2 L/min.

**Table 2.** Experiment conditions.

| Experiment | 12 July (Case A) | 29 August (Case B) |
|---|---|---|
| **Setting conditions** | • All windows open from 8:30 to 18:00<br>• Water sprinkle by mist for 5 min (0.1 L/min) at 7:00, 11:00, 15:00, and 19:00 | • All windows closed (except floor-level windows and skylight)<br>• Continuous water sprinkle by dripping from 7:00 to 19:00 (0.2 L/min)<br>• Additional plants of Japanese boxwood<br>• Water retentive block near western floor-level window |

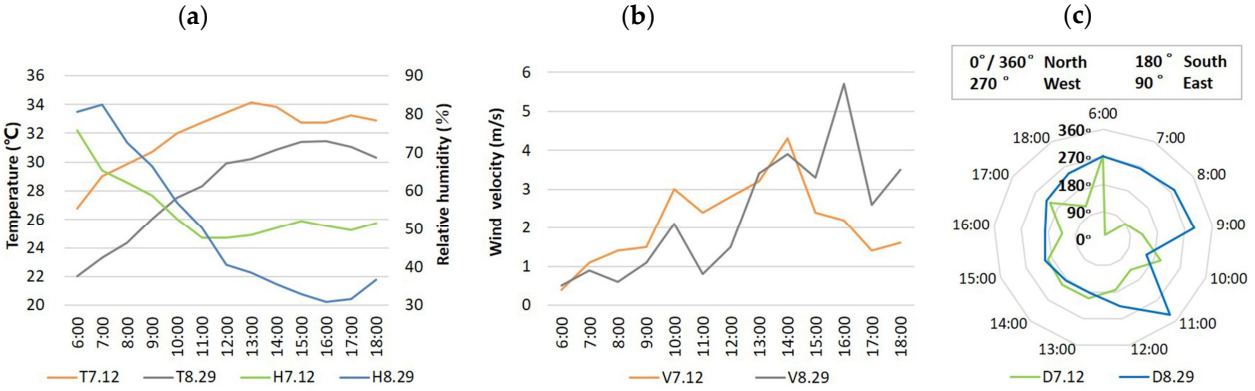



**Figure 3.** Outdoor meteorological conditions on 12 July and 29 August: (**a**) temperature and humidity; (**b**) wind velocity; and (**c**) wind direction.

#### 2.2.2. Measurement Points and Instruments

The measurement plan is demonstrated in Figure 4 and included temperature, wind velocity, and relative humidity. The vertical temperature distribution was measured across

the East–West direction of the experiment site, while considering four outdoor places (as shown in Table 3: A1–A4, GL + 0.1 m, 1.1 m), one above the water retentive block (as shown in Table 3: A5, GL + 0.5 m, 0.7 m, 1 m, 1,2 m), and three inside the house (as shown in Table 3: A6, FL + 0.2 m; A7 and A8, F. L + 0 m, 0.1 m, 0.5 m, 1.1 m, 1.8 m, 2.3 m, ceiling surface).

Relative humidity was set along with the vertical temperature distribution (as shown in Table 3: A1, A4, GL + 1.1 m; A5, GL + 0.7 m; A6, FL + 0.2 m; A7 and A8, FL + 1.1 m). Notably, MRT was also measured indoors (as shown in Table 3: A8, FL + 1.1 m).

We considered four points for wind measurement. A three-dimensional (3D) ultrasonic anemometer (A3, GL+ 0.7 m) was placed in the middle of the western path because it was important for measuring the inflow and outflow in front of the passive cooling design. Three probe anemometers were used for indoor flow velocity, which were near the western floor-level windows and at the center of the living room (as shown in Table 3: A6, FL + 0.2 m; A7 and A8, FL + 1.1 m).

**Table 3.** Measurement plan.

| | | Temperature | Relative Humidity | Wind Velocity |
|---|---|---|---|---|
| **Location and vertical distribution to measure the data** | A1, A2, A4 | GL + 0.1 m, 1.1 m | GL + 1.1 m | - |
| | A3 | GL + 0.1 m, 0.7 m, 1.1 m | - | GL + 0.7 m |
| | A5 | GL + 0.5 m, 0.7 m, 1 m, 1.2 m; | GL + 0.7 m | - |
| | A6 | FL + 0.2 m | FL + 0.2 m | FL + 0.2 m |
| | A7 | FL + 0 m, 0.1 m, 0.5 m, 1.1 m, 1.8 m, 2.3 m, and ceiling surface | FL + 1.1 m | FL + 1.1 m |
| | A8 | FL + 0 m, 0.1 m, 0.5 m, 1.1 m, 1.8 m, 2.3 m, and ceiling surface | FL + 1.1 m | FL + 1.1 m |
| **Instrument** | | **Air temperature:** 0.1-mm$\phi$ T-type thermocouple with multipoint measurement method<br>**Surface temperature:** 0.3-mm$\phi$ T-type thermocouple<br>**MRT:** 0.1-mm$\phi$ T-type thermocouple inside a globe thermometer (FL+ 1 m at A8 only) | Resistance change type (TDK, CHS-UPS) | **A3:** 3D ultrasonic anemometers<br>**A6, A7, A8:** KAJIO, DA0600 |

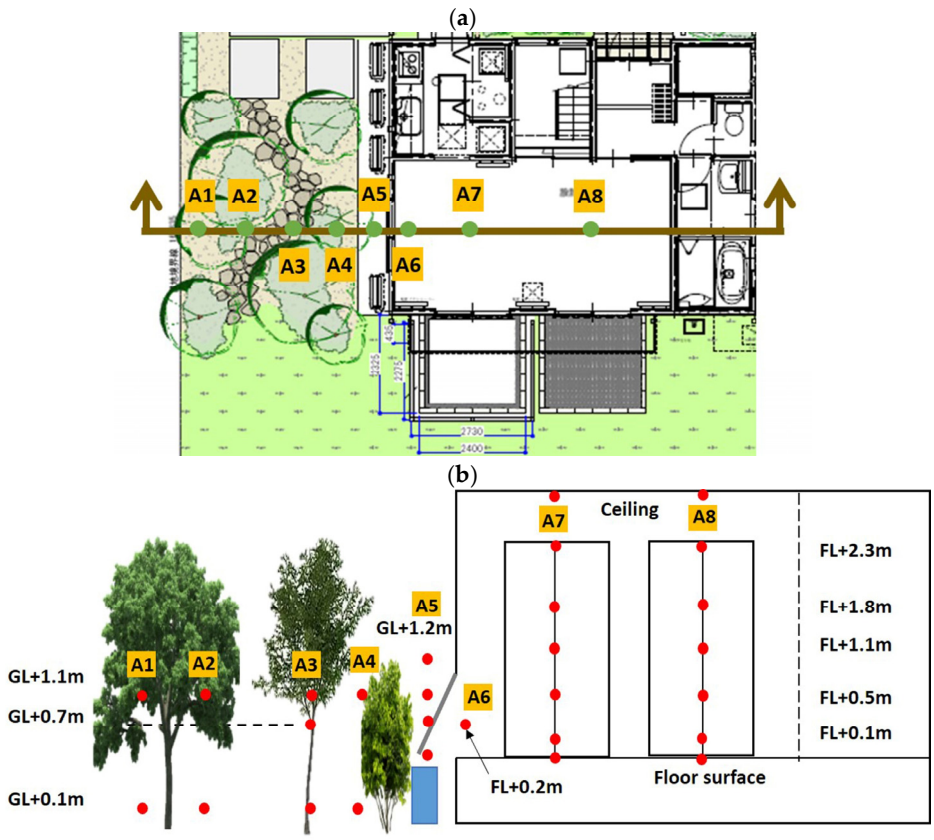



**Figure 4.** Measurement points in (**a**) horizontal and (**b**) vertical directions.

### *2.3. Computational Fluid Dynamics (CFD) Simulation*

#### 2.3.1. Simulation Method

In addition to the experiment for verifying the effect of the passive cooling design, numerical analysis is necessary for the further evaluation and improvement of cooling performance. Therefore, we performed numerical simulation to determine the air temperature, wind velocity, and humidity to investigate the influence of window design on the performance and the process of the airflow for the passive cooling design implemented in the study house.

A commercial computational fluid dynamics (CFD) software called scSTREAM Version 2020 (Cradle, Tokyo, Japan) was applied for this study. The Reynolds-averaged Navier–Stokes Simulation (RANS) model has been commonly used to address urban physical problems in CFD [30–32], and is suitable for steady-state analysis because it is based on time average. The standard K-epsilon (k-ε) turbulence model was selected, with the outdoor flow considered as high Reynolds number turbulence in the actual environment.

An important precondition in this CFD simulation assumed the airflow to be incompressible, and the air density was constant when the temperature changed. The natural flow in this case was completely under 100 m/s, and the temperature gradient was under 100 °C, which met the criterion for incompressible flow. Therefore, the governing equations in the simulation followed the steady 3D conservation equations of mass and momentum for incompressible turbulent flow, along with the equations of energy for heat.

For conservation of mass, the following equation was applied:

$$\frac{\partial u}{\partial x} + \frac{\partial v}{\partial y} + \frac{\partial w}{\partial z} = 0 \tag{1}$$

This can be written in a simplified form, as follows:

$$\nabla \cdot \nu = 0 \tag{2}$$

where $\nu$ is velocity.

The above equation reflects the fact that mass was conserved, which, flowing in and out at a controlled volume, keeps a balance.

For conservation of momentum, we applied the Navier–Stokes equations, as follows:

$$\frac{\partial \mathrm{v}}{\partial \mathrm{t}} + \nabla \cdot (\nu\nu) = -\nabla \mathrm{p} + \nabla \cdot (2\mu \mathrm{D}) \tag{3}$$

where $\partial \mathrm{v}/\partial \mathrm{t}$ is time, representing the flow change with time changing; $\nabla \cdot (\nu\nu)$ is convection, which means the change of flow due to the movement; $\nabla \cdot (2\mu \mathrm{D})$ is the pressure; and $\nabla \mathrm{p}$ is viscosity, representing the uniformity of flow by viscosity. Within the above terms, p is pressure, $\mu$ is viscosity coefficient, and D is symmetric terms of velocity gradient.

D was further calculated using the following equation:

$$\mathrm{D} = \frac{1}{2}\left\{\nabla \nu + (\nabla \nu)^{\mathrm{T}}\right\} \tag{4}$$

For conservation of energy of incompressible flow, we used the following equation:

$$\frac{\partial\left(\rho \mathrm{C_p T}\right)}{\partial \mathrm{t}} + \nabla \cdot \left(\nu \rho \mathrm{C_p T}\right) = \nabla \cdot (\kappa \nabla \mathrm{T}) \tag{5}$$

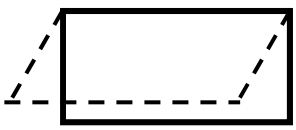
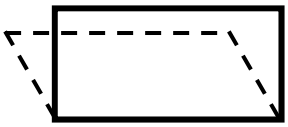
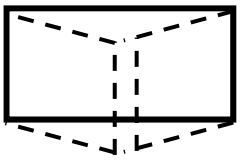
where $\nabla \cdot \left(\nu \rho \mathrm{C_p T}\right)$ is the heat convection, $\nabla \cdot (\kappa \nabla \mathrm{T})$ is the heat transfer by heat conductivity, T is temperature, $\rho$ is density, $\mathrm{C_p}$ is specific heat, $\nu$ is velocity, and k is the heat conductivity coefficient.

2.3.2. Sensitivity Analysis on the Floor-Level Window Design

According to a survey on the characteristics of natural ventilation in 62 different building types in Japan, natural ventilation using floor-level windows is as good as that achieved by high and central windows [33]. This portrays the acceptability of floor-level windows in real building design processes. As ventilation performance is closely related to window design [34,35], we can optimize the design of floor-level windows to improve the general passive cooling effect. However, it is still unclear whether existing floor-level windows can realize the best cooling performance when combined with passive cooling design. Thus, our study aimed to evaluate the influence of different window designs on ventilation and cooling performance.

Floor-level windows in the experiment house consisted of generally top hung windows, with an opening angle of 30°. The window type and opening angle were chosen as the main topics in this study. Apart from top hung windows, bottom and side hung windows are also commonly used in building window design [36]. A basic summary of all window shapes and related information are listed in Table 4. The passive cooling design for Cases 1–9 was set as the same as Case B, and the simulation settings are presented in Section 3.1.

**Table 4.** Window types and characteristics.

| Window Type | Top Hung | Bottom Hung | Side Hung |
|---|---|---|---|
| Size | 800 × 400 mm | 800 × 400 mm | 400 × 400 mm (2) |
| Figure of one unit |  |  |  |

Notably, in addition to the window type, the opening angle of the window is also an essential design parameter [37]. For a specific window type, the opening area varies in shape and surface area with increasing opening angle [38]. We considered nine testing cases, listed in Table 5, with opening angles of 30°, 45°, and 60°, in three window types. Except for the two western floor-level windows, the shape of the two northern floor-level windows were changed simultaneously. However, the window design process for the floor-level windows in this case study had a few limitations; we did not consider the interactive effects of different wind directions, window sizes, and building orientations [39].

**Table 5.** Testing cases considered in this study.

| Window Type | Opening Angle | Case |
|---|---|---|
| Top hung window | 30° | Case 1 |
| | 45° | Case 2 |
| | 60° | Case 3 |
| Bottom hung window | 30° | Case 4 |
| | 45° | Case 5 |
| | 60° | Case 6 |
| Side hung window | 30° | Case 7 |
| | 45° | Case 8 |
| | 60° | Case 9 |

2.3.3. Investigation on Cooling Effect by Passive Cooling Design

In order to evaluate the passive cooling effect on the semi-outdoor and indoor thermal environments by using simulation, in addition to the experiment, a comparison between the case with and without passive cooling design was taken into consideration. Case 0 was set

as the same as Case 1, except for passive cooling design (i.e., plants, water retentive block, and dripping pipe), the purpose of which was to observe the original thermal environment without the passive cooling design.

### *2.4. Calculation of Standard Effective Temperature* (SET*)*

With the passive cooling design, all the environmental parameters, such as radiant temperature, humidity, wind velocity, etc., change simultaneously; SET* was thus selected in Sections 4.1.2 and 4.2.3 to estimate the thermal comfort, considering the thermal environments under different conditions by being changed from that under the standard environment.

For most cases, the comfortable temperature range was 22.2–25.6 °C with regard to the SET*, which varied depending on different genders or races [40]. The SET* is calculated following the standard calculation conditions, where the metabolic rate of 1.0 met and clothing of 0.5 clo is fixed, while the temperature, wind velocity, and relative humidity are determined by the simulation results. The mean radiant temperature (MRT) is indispensable in the calculation of SET*, but was difficult to measure directly in this case because radiation was excluded in the simulation. Referring to the experiment conducted by Haramoto [41], the deviation between air temperature and MRT was around 0.501 °C; the approximate value of MRT was estimated using the following equation:

$$\mathrm{MRT} = \mathrm{T_{air}} + 0.5 \quad (6)$$

where $\mathrm{T_{air}}$ is air temperature (°C).

## 3. Validation of Computational Fluid Dynamics (CFD) Simulation for Passive Cooling Design

Due to the similar outdoor environment, meteorological conditions, and microclimate, the validation method in this study followed the one conducted by Del Rio et al. [42], which adopted the CFD-based simulation method to observe the cross-ventilation performance by large openings. Different from their case, the humidity conditions were added to be tested in our validation, and the input relative humidity as the boundary condition was observed in the experiment. In addition, the thermal comfort in terms of SET* was also evaluated based on the CFD-based simulation results.

The experiment results at 12:00 on 29 August 2014 were selected as the validation case in this study. Figure 5 illustrates the 3D model of the entire experiment site. Inside the house, the floor plans of the first and second floors were based on the real layout of the house, with all the doors kept closed, except for the sliding door in the stair hall.

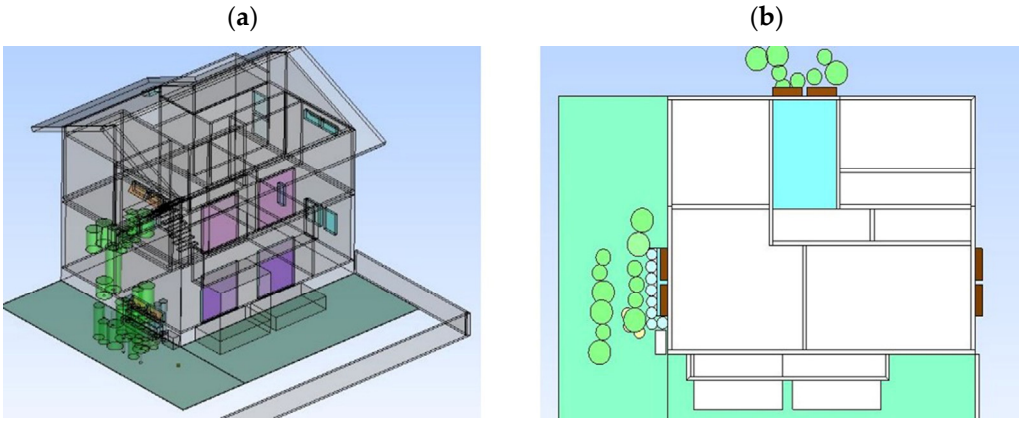



**Figure 5.** (**a**) Three-dimensional (3D) model of the experiment house, and (**b**) its surroundings.

To validate the reliability and quality of the simulation model applied in this study, the simulation results of the validation case were compared with the experiment data, in

terms of the indoor and outdoor air temperature, wind velocity, and relative and absolute humidity at the set measurement points, as shown in Figure 4.

### *3.1. Simulation Conditions*

#### 3.1.1. Calculation Setting

Table 6 illustrates a brief introduction to the calculation conditions of our study in the validation case. In the study house, the windows were open toward the prevailing wind direction and there were no shielding objectives nearby. The decision of the 3D computational domain was mainly based on the guidelines provided by the Architectural Institute of Japan (AIJ) [30] and domain dependency studies. It is highly recommended to maintain a height of 2.3–5 H, 10–15 H, and 5–6 H from the model to the inflow, outflow, and top boundaries, respectively, where H represents the height of the building model [43,44]. For the validation case, 5 H for inflow boundary, 15 H for outflow boundary, and 5 H for top boundary were set.

The computational grid consisted of hexahedral cells of size 100 × 100 × 100 mm, 251 × 269 × 165 = 11,140,635 meshes in total, and a maximum stretching ratio of 1.1.

**Table 6.** Calculation conditions of this study.

| | | |
|---|---|---|
| **Domain** | | 174.5 × 174.5 × 41.5 m |
| **Mesh** | | 251 × 269 × 165 = 11,140,635 |
| **Turbulence model** | | Standard k-ε model |
| **Inflow boundary** | **Direction** | SW (229°) |
| | **Velocity** | 1.5 m/s (Basic height: 8.3 m) |
| | **Environment** | III: Urban area formed by small buildings<br>ZG: 450 m α: 0.2 |
| **Outflow boundary** | | $Y_{max}$ and $X_{min}$: No pressure |
| **Wall boundary** | | $Z_{min}$: No slip; $Z_{max}$: Free slip |
| **Scheme for convection terms** | | QUICK scheme |
| **Cycle** | | Stable analysis, 500 cycle |

#### 3.1.2. Flow Conditions

The wind velocity at 12:00 on 29 August was 1.5 m/s from south-west, according to the weather station. The actual angle of wind was 229° (N: 0°, E: 90°, S: 180°, W: 270°), while the study house was facing 40° west of south (220°); therefore, the inflow direction was set with an angle of 9° to the study house. The house model was built facing due south (180°) in simulation, and the inflow direction was kept 9° from due south (189°) to recreate the actual inflow condition. Figure 6 illustrates the angle formed between the study house and inflow, along with the inflow direction settings applied in the simulation model.

The wind profile followed power law because the surrounding environment influences the wind velocity. Regarding the input of the surface roughness type for simulation, the urban area of small houses was selected because the study house was located in a residence area mainly formed by low-rise houses. Under such conditions, the inflow exponent value was considered to be 0.2, and the height of the ground layer was considered as 450 m.

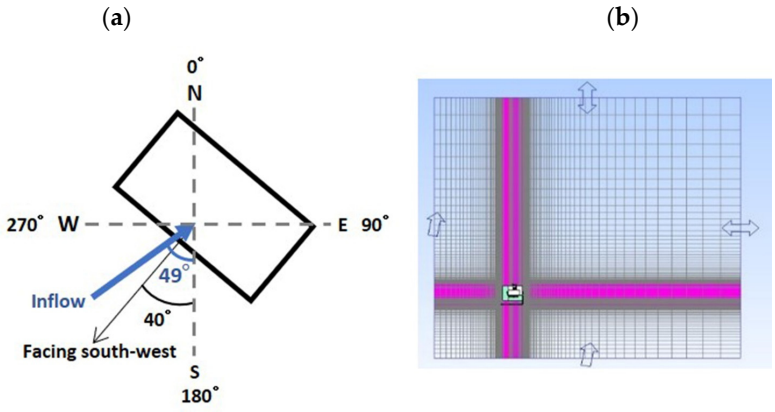



**Figure 6.** Flow conditions of the experiment and simulation conducted in this study: (**a**) direction of the inflow; (**b**) computational grids.

3.1.3. Thermal Conditions

With respect to the temperature data from thermal images, the heat transfer calculation was mainly related to the convective heat transfer coefficient and the surface and initial temperatures.

All thermal boundary layers were set as adiabatic to ensure no heat transfer between the analysis domain and external space. The surface temperature depended on the thermal images captured using an infrared camera (Model: Thermo GEAR G100, Nippon Avionics Co., Ltd., Kanagawa, Japan) during the experimental period; a summary of the registered surfaces and temperatures at 12:00 on 29 August is provided in Table 7.

To calculate the heat transfer between air temperature and the registered surface, there is no need for conductivity and radiation heat transfer. The specific convective value varied in outdoor and indoor spaces, and was calculated using the Jürges equation [45], as follows:

For normal surfaces in outdoor environment:

$$\begin{cases} \alpha_{cv} = 5.6 + 3.9V \ (V \leq 4.9 \ m/s) \\ \alpha_{cv} = 7.2V^{0.78} \ (V \geq 4.9 \ m/s) \end{cases} \quad (7)$$

where $\alpha_{cv}$ is specific convective value, and V is wind velocity (m/s).

**Table 7.** Indoor and outdoor surface temperature.

| Indoor Surface Temperature (°C) | | Outdoor Surface Temperature (°C) | |
|---|---|---|---|
| Indoor wall (South, East) | 27.8 | Outdoor wall (upward of West wall) | 36.54 |
| Indoor wall (North, West) | 28.04 | Outdoor wall (downward of West wall) | 34.89 |
| Ceiling of the 1st floor | 26.47 | Outdoor wall (North, East wall) | 34 |
| Ground of the 1st floor | 27.59 | Outdoor wall (South wall) | 37 |
| Sweeping windows | 30.34 | Roof | 42 |
| | | Water retentive block | 26 |
| | | Ceramic grid panel | 34 |
| | | Outside step (West, East) | 32, 52 |
| | | Outdoor louver | 23.8 |
| | | Outdoor shading | 47 |

3.1.4. Canopy Setting

Plants in the field experiment included trees, shrubs, and grass. Trees consisted of trunk and foliage, which could be regarded as obstacle and porous material, respectively, and attributes resistance characteristics to the trees. Shrubs are generally short and covered by leaves, without long trunks; in our study, the shrub and grass models were set as porous material. According to the characteristics of different plants, the plant models were mainly divided into three types, as shown in Figure 7; tree foliage, shrubs, and grass were considered as porous materials and tree trunks were considered as obstacles.

Figure 8 illustrates the plant distribution of different species in the experiment site, and their detailed characteristics are summarized in Table 8. To ensure the accuracy of the plant model, we determined the plant properties, such as the leaf area density (LAD) and drag coefficient (Cd). LAD is mainly used to understand the vertical 3D structure of one plant in a horizontal layer, which is defined as the ratio of the total one-sided leaf area per unit to the layer volume [46]. In some cases, it reflects the rate of photosynthesis. Notably, the LAD of different plants used in this study were mainly based on the measurement data from a previous site experiment [47].

The Cd was calculated by measuring the resistance force, LAD, and inflow velocity. The value of drag coefficient was based on a wind tunnel experiment conducted by Kamiyama [48], which followed the formula of resistance, as follows:

$$F_d = \frac{1}{2}\rho a C_d V^2 \quad (8)$$

where ρ is air density ($kg/m^3$), a is representative area ($m^2$), $C_d$ is drag coefficient, and V is wind velocity (m/s).

To calculate the heat transfer between the plants and air, it is significant to calculate the convective heat transfer coefficient of the plants. The convective heat transfer coefficient (CHTC) is an index that represents the sensible heat transfer between foliage and air, which is governed by the leaf shape, leaf size, and ambient flow field. It can be calculated according to the formula applied by Asawa [49], as follows, representing the CHTC in the crown part:

$$\mathrm{CHTC} = 7.9\mathrm{V} + 17.2 \quad (9)$$

where V is wind velocity (m/s).

When the outdoor wind velocity was 1.5 m/s, the CHTC value was approximately 29 $\mathrm{W/m^2 \cdot K}$.

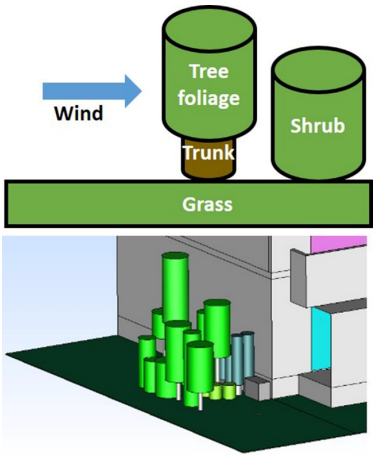



**Figure 7.** 3D model of plants.

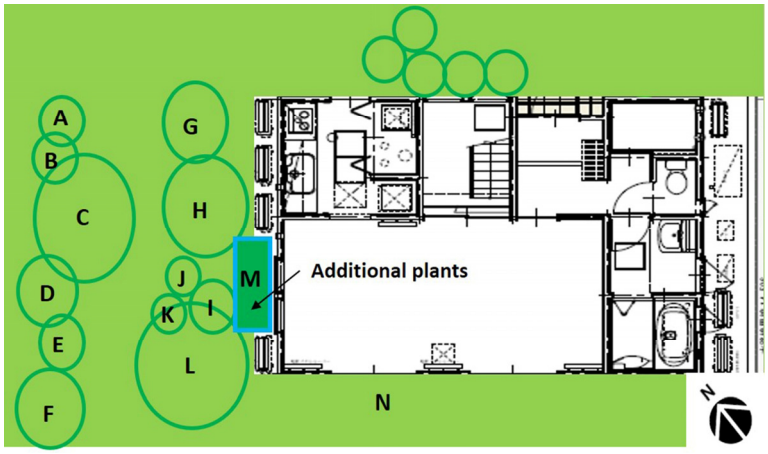



**Figure 8.** Plant distribution at the experiment site. Letters (A, B, etc.) refer to Table 8.

**Table 8.** Plant characteristics analyzed in this study.

| Types | Number Shown in Figure 8 | $C_d$ | LAD ($m^2/m^3$) | Temperature (°C) |
|---|---|---|---|---|
| Evergreen shrub | A | 0.5 | 5–6 | 29.15 |
| Evergreen tree | D, I, L | 0.6 | 5–6 | 34.23 |
| Delicious shrub | B, C, F, J, K | 0.6 | 3–5 | 29.15 |
| Delicious tree | E, G, H | 0.6 | 3–5 | 34.23 |
| Grass | N | 0.8 | 7 | 37 |
| Boxwood | M | 0.5 | 5–6 | 28 |

Note: leaf area density (LAD).

#### 3.1.5. Humidity Conditions

With the passive cooling design near floor-level windows, the humidity conditions in the house changed under the influence of additional moisture sources, such as plants, water retentive blocks, and dripping pipes.

The moisture diffusion coefficient of plants was calculated by multiplying the transpiration rate and leaf area. The transpiration rate of irrigated plants generally reaches a peak value around noon or in the afternoon on a sunny summer day. At 12:00, the peak value of irrigated plants is approximately 1 kg/m$^2$·h on a sunny day, with sprinkling [50]. The leaf area of the plants in the experiment was measured on site [47]; the value was 0.67 m$^2$ for oak trees and 0.582 m$^2$ for boxwood.

Water retention value is the key factor in evaluating the evaporation rate of the water retentive block, which consists of a concrete block of high water-absorbing quality. According to a fundamental study on this material, the evaporation rate was around 0.7 kg/m$^2$·h at 12:00 on a sunny day [27]. Notably, in our study, the block was a rectangular panel with a length of 1.7 m, a width of 0.3 m, and a total surface area of 0.51 m$^2$.

The dripping pipes consisted of sprinkling points, with the total dripping rate being 12 kg/h. One pipe was set at GL + 1 m to cover the plants, and the other was placed next to the water retentive block.

The relative humidity was measured on site, but the absolute humidity could not be measured directly. Thus, the absolute humidity was calculated by mutually transformational conditions with relative humidity; the formula was mainly based on the tutorials of Cradle CFD 2020-csSTREAM [51], as follows:

$$\mathrm{Rh} = \mathrm{Ah} \times \frac{\mathrm{P/E}}{0.622 + \mathrm{Ah}} \tag{10}$$

where Rh is relative humidity (%), Ah is absolute humidity (g/kg), P is atmospheric pressure (hPa), and E is saturated vapor pressure (hPa).

Under standard atmosphere pressure, it is generally 1013.25 hPa. Saturated vapor pressure was calculated by the formula of Tetens [52], as follows:

$$\mathrm{E} = 6.11 \times 10^{\frac{7.5t}{t+237.3}} \tag{11}$$

where t is air temperature (°C).

### *3.2. Validation Results*

The measurement points generally agreed with respect to the simulation results, as shown in Table 9; the determination value ($R^2$) was 0.95–0.99, and the absolute humidity was 0.94. The root mean square error (RMSE) was generally lower than 0.33 °C and 0.48 g/kg for the vertical temperature and the absolute humidity, respectively. Hence, the validation case was considered to represent the same experiment conditions in the simulation.

Figure 9 illustrates the comparison of wind velocity in the experiment and the simulation. The wind velocity showed good consistency, with a $R^2$ of 0.99 and a RMSE of 0.02 m/s. When comparing the outdoor wind velocity (A3) with indoor flow velocity (A6), strong wind shielding occurred in the passive cooling design space. Figure 10a compares the outdoor vertical temperature in front of the floor-level windows, and Figure 10b represents the horizontal temperature distribution across the experiment site; the results exhibited a consistent changing trend in the two directions. Notably, the vertical temperature at lower positions (0.5 and 0.7 m) were much lower than for ambient air, revealing the cooling effect of the passive cooling design in front of the floor-level windows. The maximum error among all the temperature points was at A5 (GL + 0.7 m) of 0.6 °C, but it did not affect the model validity significantly, considering the general tendency and deviation. Regarding the MRT, it also shows an acceptable error of around 0.4 °C between the experiment and simulation.

Figure 11a,b illustrate the horizontal relative humidity and absolute humidity distribution in the study area, respectively. The relative humidity for $R^2$ was 0.98; however, the value was lower, at 0.94, for the absolute humidity. The errors occurred at the A5 and A6 near floor-level windows. Notably, the actual humidity environment was more complicated than the simulation setting. For instance, it was hard to measure the evaporation of the ground and drips on new planted boxwood precisely in the field experiment. Such factors related to moisture content were omitted in the boundary condition setting. Thus, the general outdoor absolute humidity in the simulation was lower than that in the experiment; in particular, the maximum deviation was 0.86 g/kg at A6. In addition, the error at A5 was 0.62 g/kg, while it does not show obviously in relative humidity. This can be attributed to the temperature difference at the same measurement point, because generally, a lower temperature in the simulation leads to a simultaneous rise in the relative humidity.

**Table 9.** Correlation and deviation between the measured and simulated results.

| Index | MSE | RMSE | $R^2$ |
|---|---|---|---|
| $T_V$ | 0.11 °C | 0.33 °C | 0.95 |
| $T_H$ | 0.10 °C | 0.32 °C | 0.98 |
| Wind velocity | 0.0004 m/s | 0.02 m/s | 0.99 |
| Relative humidity | 2.5% | 16% | 0.98 |
| Absolute humidity | 0.23 g/kg | 0.48 g/kg | 0.94 |

Note: leaf area density (LAD); mean square error (MSE); root mean square error (RMSE); R-squared ($R^2$).

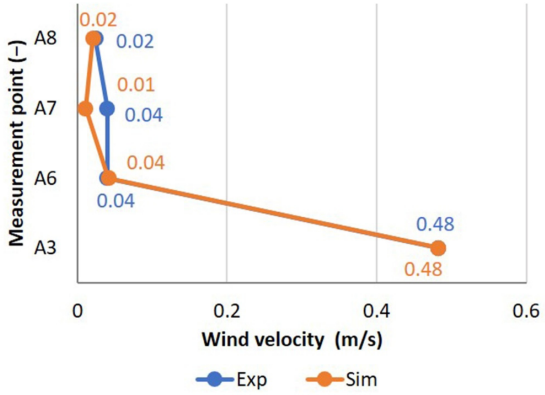



**Figure 9.** Distribution of measured and simulated wind velocity. Exp (blue line) stands for the data measured in experiment, while Sim (orange line) stands for the data obtained by simulation.

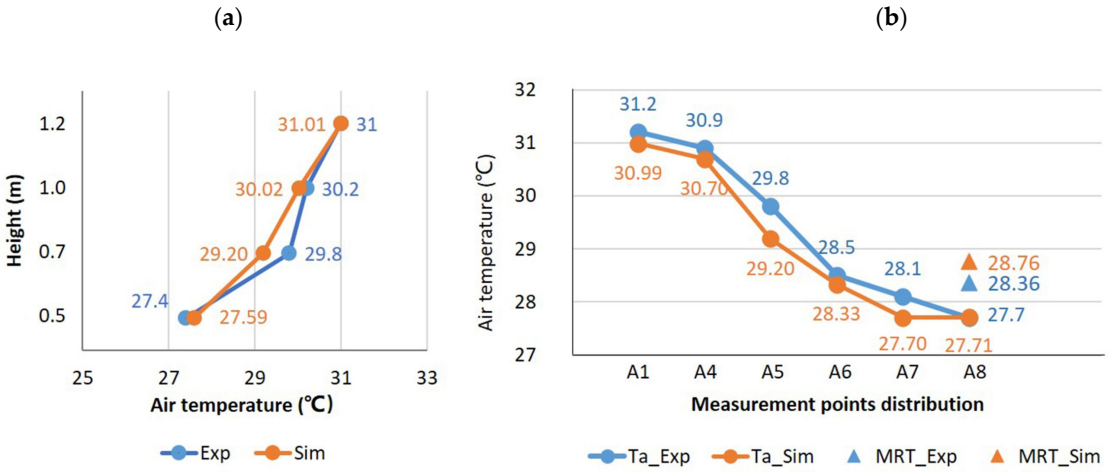



**Figure 10.** Distribution of measured and simulated temperature: (**a**) vertical Ta distribution at A5, and (**b**) horizontal Ta distribution at GL/FL + 1.1 m and MRT at A8, FL + 1.1 m.

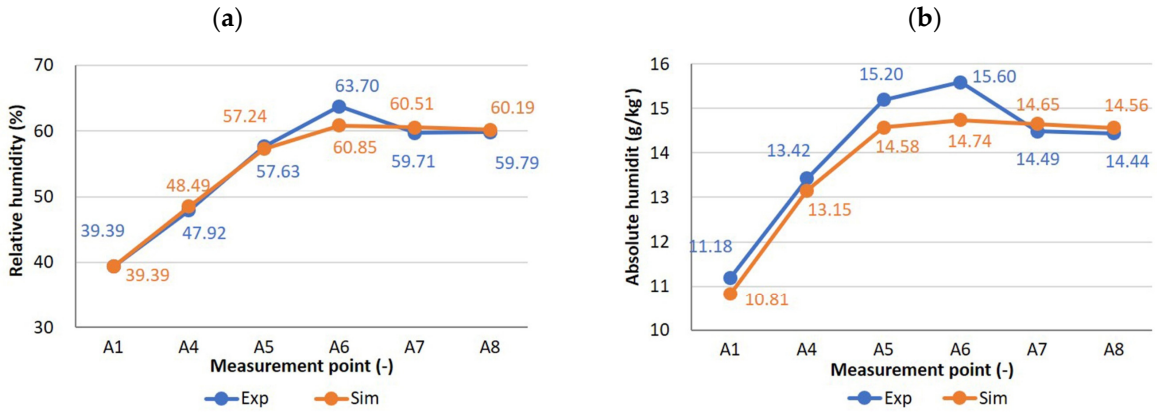



**Figure 11.** Distribution of measured and simulated humidity: (**a**) horizontal relative humidity distribution, and (**b**) horizontal absolute humidity distribution.

## 4. Result and Discussion

### *4.1. Investigation of Cooling Effect by Passive Cooling Design*

#### 4.1.1. Experiment Results and Analysis: Temperature and Humidity Distribution

Figure 12a illustrates the outdoor vertical temperature distribution in front of the floor-level windows. In Case A, there was no obvious change in the vertical direction. Conversely, in Case B, we observed a significant temperature difference with the passive cooling design. With the increase in air temperature in the afternoon, the difference at a lower position was more obvious. Considering that the outdoor air temperatures on 29 August (experiment day for Case A) kept increasing from noon to afternoon and its wind velocity was generally lower than that on 12 July (Case B), the influence of the weather should not be the driven cause for the more obvious descending trend of the temperatures near the floor-level windows in Case A. Thus, it can be suggested to be due to the stronger cooling effects of evaporation and transpiration.

As demonstrated in the thermal images captured near the floor-level windows of Case B (Figure 13), both the surface temperatures of the plants and the water retentive block were lower than the air temperature. According to the results at 15:00, the cooling area expanded, with a maximum difference of 7 °C. Therefore, the passive cooling effect on the semi-outdoor space was confirmed in front of the floor-level windows. Figure 12b illustrates the horizontal temperature distribution in the East–West direction across the experiment site. The downtrend from the outdoor to indoor temperatures was comparatively evident in Case B, especially from A4 to A5, which provided credible proof that the passive cooling design affected the indoor space. In conclusion, the passive cooling design improved the indoor and semi-outdoor environments in terms of temperature, and the descending trend of temperature was gradual in the further indoor space.

With the passive cooling design, the humidity condition changed, as illustrated in Figure 14; moisture sources, such as sprinkling pipes and additional plants, were set in the experiment. In Case A, the outdoor relative humidity gradually increased from A1 to A5, and it decreased at A6, portraying a downward trend deeper inside the house. Relative humidity portrayed a similar change in the outdoor space, while the indoor relative humidity at A6 portrayed a steady increase in Case B, due to the passive cooling design in front of the floor-level windows. By comparing the different tendencies from A5 to A6 in the two cases, we concluded that the passive cooling design influenced the surrounding humidity change.

#### 4.1.2. Simulation Results and Analysis: Temperature, Flow, Humidity, and Standard Effective Temperature* (SET*)

The simulated vertical temperature distributions of Case 0 and 1 at 12:00 on 29 August are shown in Figure 15a. It should be noticed that huge temperature differences exist in front of the floor-level windows, particularly near the surface of the water retentive

block where the maximal temperature difference is more than 3 °C at GL + 0.5 m. This verified that the semi-outdoor space in front of the floor-level windows was cooled off by the passive cooling design. However, the water retentive block hardly affected higher space at a height of 0.2 m above the height of block surface (GL + 0.5 m), since the temperature difference at GL + 1 m was smaller than those at lower points, as shown in Figure 15a; it was mainly influenced by the plants and dripping pipe. Regarding the horizontal temperature distribution, as shown in Figure 15b, the temperature of Case 1 decreases sharply from the measurement point of A4 to A5; the difference from that of Case 0 is more than 1.5 °C at A5. Regarding the temperature distribution across the house of Case 1 and Case 0, as illustrated in Figure 15c,d, respectively, the indoor temperature in the middle of the living room of Case 1 is lower than that of Case 0 by about 0.4 °C. Thus, the passive cooling design was confirmed to be effective in reducing the temperature.

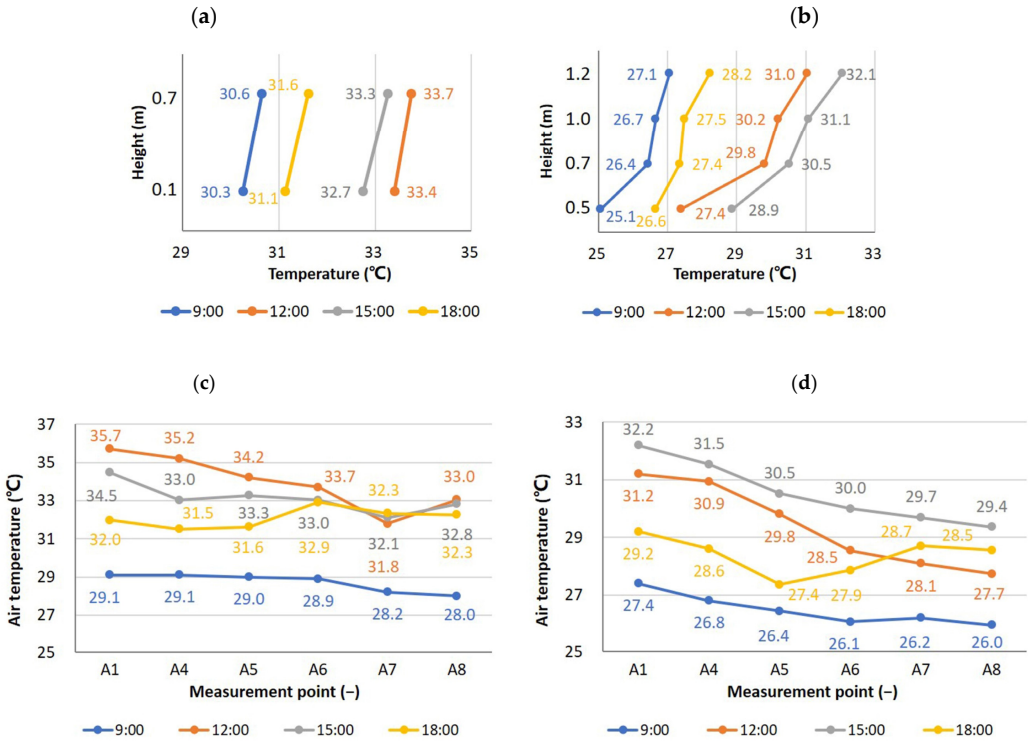



**Figure 12.** Experiment results in terms of the distribution of air temperature: vertical Ta distribution in Cases (**a**) A and (**b**) B; and horizontal Ta distribution in the East–West direction in Cases (**c**) A and (**d**) B.

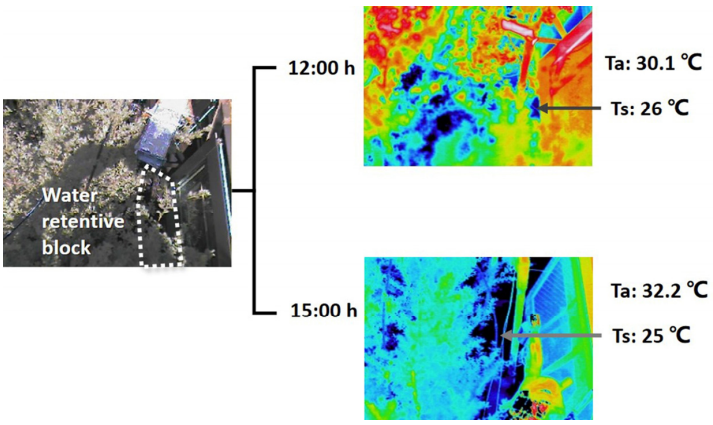



**Figure 13.** Thermal images for the water retentive block (a mitigation measure shown in Figure 2) at 12:00 and 15:00 on 29 August.

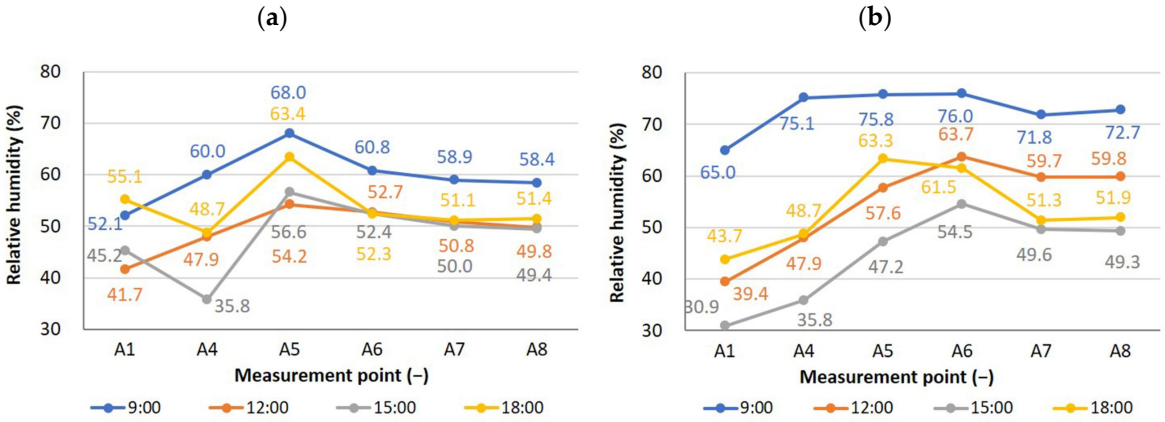



**Figure 14.** Experiment results in terms of relative humidity distribution in the East–West direction for Cases (**a**) A and (**b**) B.

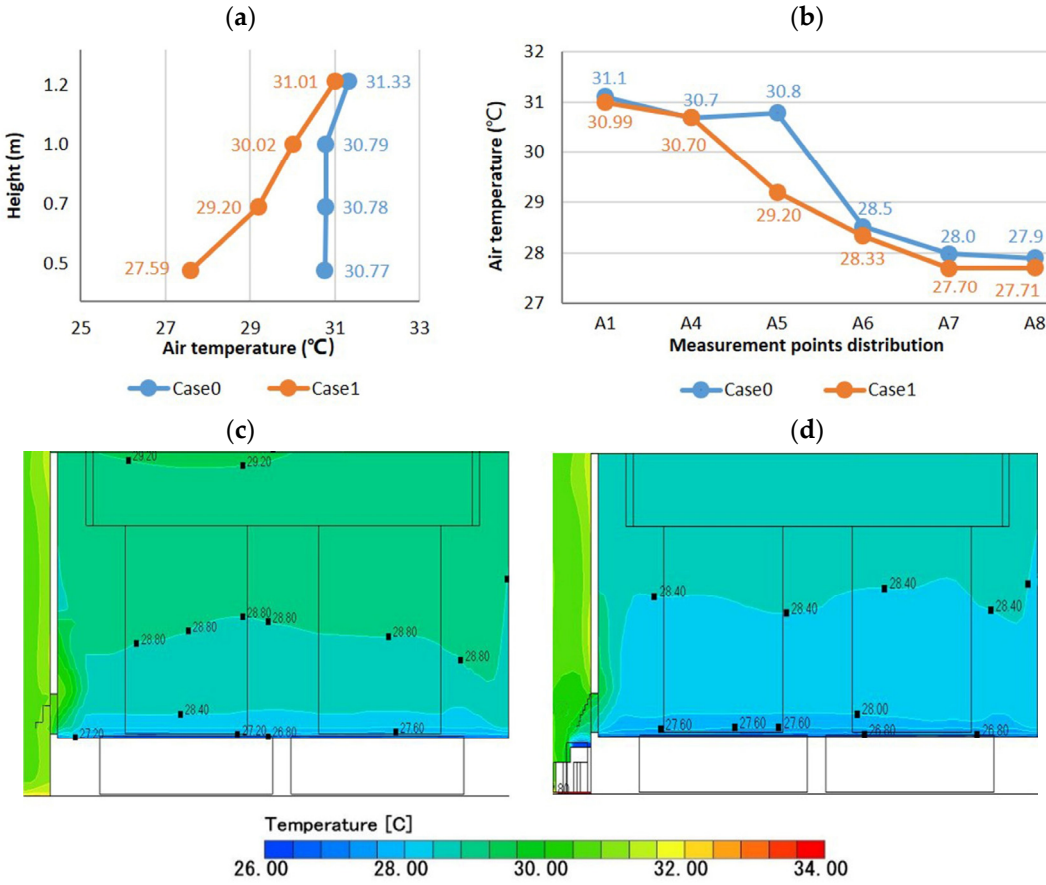



**Figure 15.** Simulation results in terms of the temperature distribution: (**a**) vertical Ta distribution in Cases 0 and 1; and (**b**) horizontal Ta distribution in the East–West direction for Cases 0 and 1; and spatial Ta distribution across the study house in the East–West direction for Case 0 (**c**) and Case 1 (**d**).

Compared with Case 0, the relative humidity increases largely in Case 1 with the transpiration of plants and the evaporation of the water retentive block with the dripping pipe, as shown in Figure 16. However, the increase of relative humidity could not be simply attributed to the increase of moisture source. As the relative humidity is highly related to the temperature, a lower temperature of Case 1 would also contribute to the increase of its relative humidity, even though its absolute humidity is constant. As shown in Figure 16, relative humidity suddenly drops at A5 in Case 0, while its air temperature rises (Figure 15b) due to the solar radiation introduced through the windows without the

plants shielding in Case 1. Meanwhile, due to the warmer air temperature, the relative humidity would decrease.

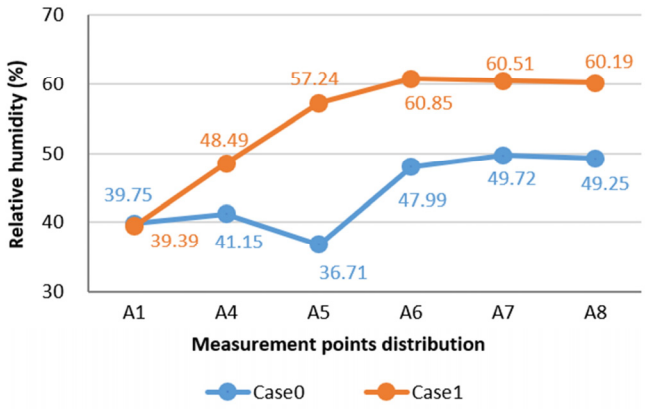



**Figure 16.** Simulation results in terms of the relative humidity in the East–West direction for Cases 0 and 1.

The flow distribution across the study house, including the distribution of wind velocity and direction, is demonstrated in Figure 17. As shown in Figure 17c,d, outdoor flow is introduced inside by western floor-level windows, and an upward moving trend of inflow can be confirmed in both Case 0 and Case 1. The indoor air flow is quite weak, apart from the space near floor-level windows, as illustrated in Figure 18a,b, since the inflow from floor-level windows is hard to reach deeper inside the living room. The inflow velocity near the floor-level windows in Case 1 is obviously lower than that of Case 0, as shown in Figure 18a,b, which is caused by the wind shielding effect of plants in the passive cooling design.

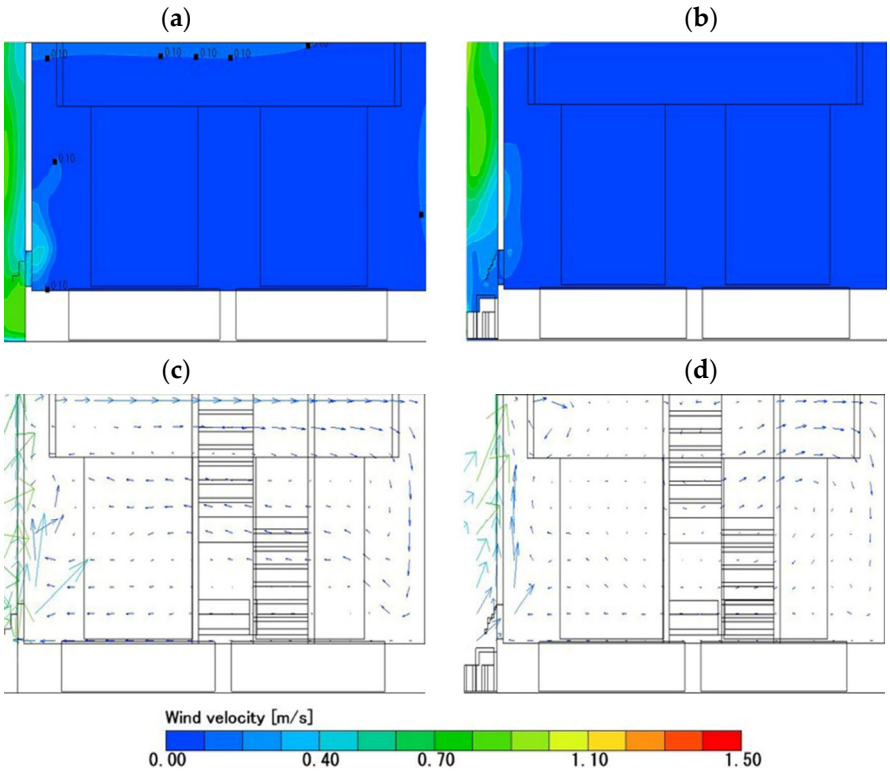



**Figure 17.** Simulation results in terms of the detail flow distribution in the East–West direction: (**a**) wind velocity in Case 0; (**b**) wind velocity in Case 1; (**c**) wind direction in Case 0; and (**d**) wind direction in Case 1.

Figure 18 shows the indoor SET* distribution in Cases 0 and 1. It demonstrates that the indoor thermal comfort could not be expected since all the SET* values exceed the upper limit of the comfort range (i.e., 25.6 °C). With the passive cooling design, the results seem to be even worse regarding the thermal comfort, particularly at A6. For indoor measurement points, there is only a minor difference between the SET*s in Case 0 and those in Case 1, indicating that the effect of wind velocity can be ignored here regarding the thermal comfort. Although it was confirmed that air temperature could be reduced by passive cooling methods, the thermal comfort of the indoor environment would not be improved. The larger variation of the East–West distribution of relative humidity of Case 1 compared to Case 0 by 10% (as shown in Figure 16) may account for this issue. Even though the air temperature decreases with the passive cooling design, the change of humidity conditions also has a large influence on thermal comfort, particularly the negative effect of increasing humidity.

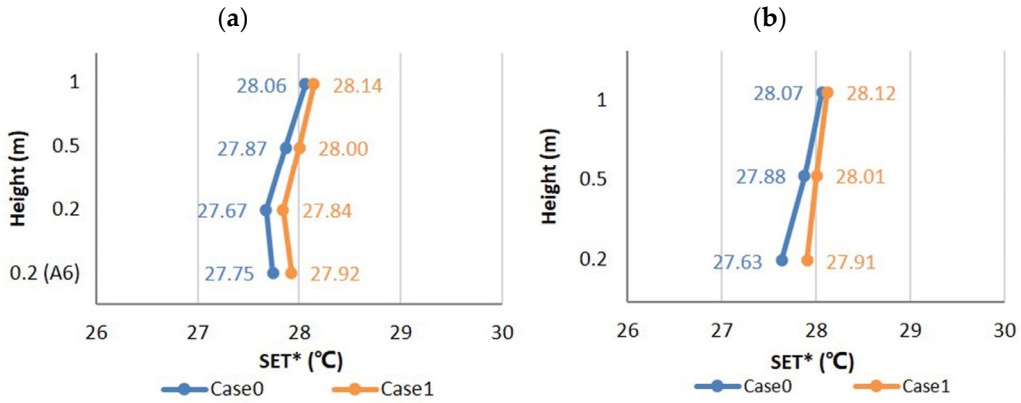



**Figure 18.** Evaluation results in terms of SET* in the west (height of GL + 0.2, 0.5, and 1 m at A7 and height of GL + 0.2 m at A6, (**a**)) and the east (height of GL + 0.2, 0.5, and 1 m at A8, (**b**)) for Cases 0 and 1.

### *4.2. Sensitivity Analysis on the Floor-Level Window Design*

#### 4.2.1. Simulation Results and Analysis: Flow Distribution

According to the horizontal flow distribution at FL + 0.2 m shown in Figure 19a, the airflow was induced by western floor-level windows, turned around in the middle of the living room, and escaped from the northern floor-level windows. As shown in Figure 19b, the inflow from the western floor-level windows exhibited an upward moving trend, which could explain the weak airflow near the floor ground. The flow near the floor was generally quite weak, below 0.1 m/s, particularly in the center of the living room. As the new planted boxwood in the passive cooling design encircled the floor-level windows, it was highly possible that the inflow velocity was reduced because of the wind shielding effect. In addition, the outflow tended to be stronger in the stair hall compared to the inflow, which may be related to the skylight.

Figure 19c portrays the indoor vertical flow distribution in the South–North direction. Notably, the airflow also entered inside from the skylight when only floor-level windows and the skylight were kept open during the experiment period. The reason for this could be attributed to the backflow forming behind the study house. Based on the analysis of the wind environment, although airflow through the passive cooling design was introduced inside by the floor-level windows, the flow hardly reached the further indoor space, resulting in an unideal cooling effect. Consequently, it is important to find a way to introduce more cooling air inside to improve the thermal environment, and the floor-level window design is regarded as an efficient way to achieve this.

The influence of window design on the cooling effect by the passive cooling design was significant.

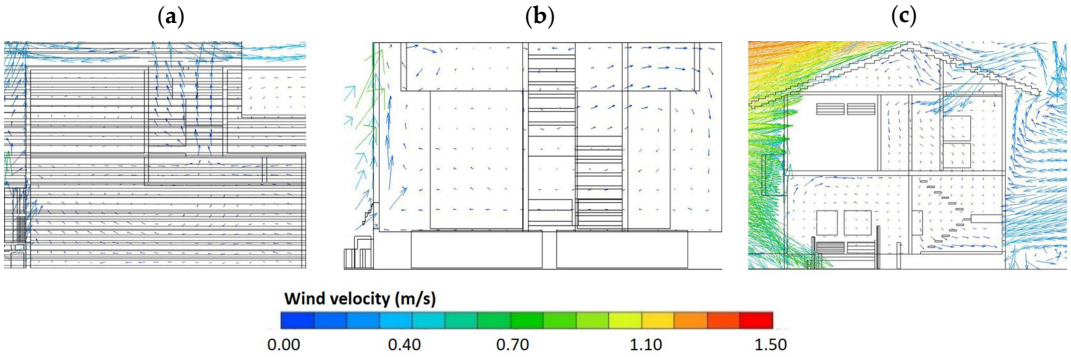



**Figure 19.** Simulation results in terms of the detail flow distribution: (**a**) horizontal flow distribution at FL + 0.2 m; (**b**) vertical flow distribution in the East–West direction; and (**c**) vertical flow distribution in the North–South direction.

#### 4.2.2. Simulation Results and Analysis: Wind Velocity

Figure 20 demonstrates the wind environment of the living room in the East–West section. With respect to different window designs, we did not observe a great influence on the center of the living room, and hardly any in the east area of the house. Regarding the wind velocity near the floor-level windows, we observed an increase with the opening angle in the top hung and side hung windows. When the opening angle was fixed, it was conspicuous that side hung windows performed better in introducing airflow than other window types. Case 9 portrayed the best ventilation performance, with large amounts of outdoor flow entering further inside, and a more active general flow movement, compared to other cases. We observed a flow to the upper areas, forming a backflow in the west. Regarding the influence on indoor flow distribution, in this case, the side hung windows with an opening angle of 60° were recommended for floor-level windows. Even though a relatively large opening angle of 60° was suggested here, a floor-level window with a limited size (800 × 400 mm in this case) would still guarantee the safety and privacy of the householders.

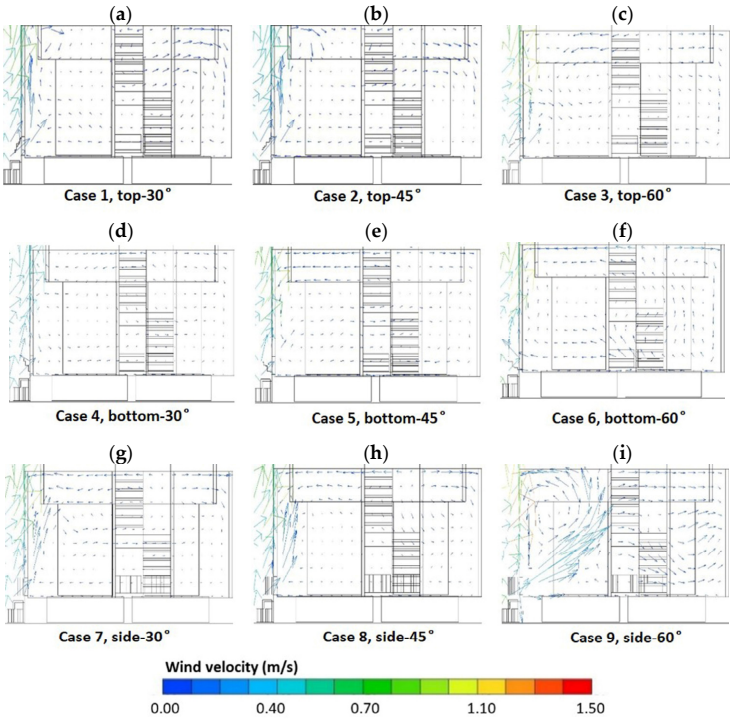



**Figure 20.** Simulation results regarding the wind environment of the living room in the East–West section for window designs for (**a–i**) Cases 1–9.

However, it was difficult for bottom hung windows to introduce airflow inside, under the same environment conditions, in Cases 4, 5, and 6. The wind velocity near the western floor-level windows was nearly zero and was weak, compared with the validation case. Particularly in Case 6, the indoor airflow escaped from the living room to outside through the floor-level windows. This indicated that bottom hung windows may not be an ideal choice for the study house.

#### 4.2.3. Simulation Results and Analysis: Standard Effective Temperature* (SET*)

The indoor SET* in the west (A6 and A7, shown in Figure 4) and east (A8, shown in Figure 4) of the living room is illustrated in Figure 21. For all cases, the SET* values were around 28 °C and above the upper limit of the comfort range. As the outdoor meteorological conditions at 12:00 are not ideal in summer, it was difficult to generate a large enough cooling effect. In the center of the living room, the SET* at a lower space was generally lower than that at a higher space, which suggested the effect of floor-level windows on the indoor environment.

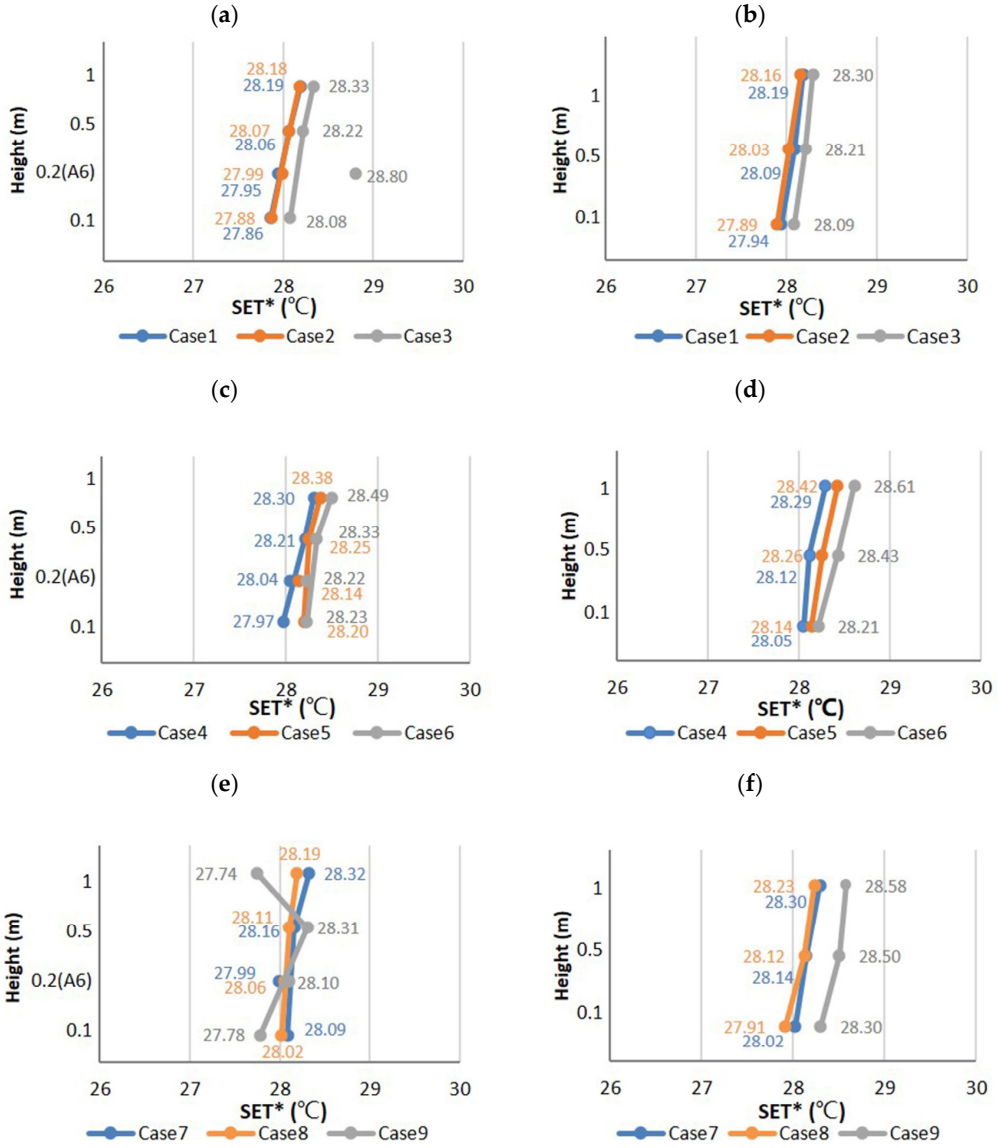



**Figure 21.** Evaluation results in terms of SET* in the west (height of GL + 0.1, 0.5, and 1 m at A7 and height of GL + 0.2 m at A6, left column, (**a**,**c**,**e**)) and the east (height of GL + 0.1, 0.5, and 1 m at A8, right column, (**b**,**d**,**f**)) for different window designs, for Cases 1–9.

Among the three window types in this study, there was no obvious difference in the SET* distribution. Although bottom hung windows did not ventilate the house effectively, the general cooling performance was not affected. When the window type was fixed, the opening angle did not portray great influence on the SET* between small angles, such as 30° and 45°. At an opening angle of 60°, a stronger but negative impact on the indoor thermal environment was observed, especially in the east of the living room. As mentioned above, the wind velocity increased with the opening angle of the windows, and hotter outdoor airflow at 12:00 could enter the house, which reduced the thermal comfort of the indoor environment.

Case 9 portrayed the best results in terms of ventilation performance; however, the general indoor thermal environment did not improve with stronger inflow, except near the floor-level windows. Especially in the east, the SET* vertical distribution of Case 9 showed a sharp rise, which was not consistent with the situation in the west. However, the thermal comfort near the floor-level windows could be improved if the wind velocity was high enough; the inflow temperature did not decrease, even after using the passive cooling design.

As a conclusion, regarding the type of floor-level windows, the side hung type performed best in introducing airflow inside the house; moreover, an opening angle of 60° appears to be the best choice, in terms of an obvious enhancement of ventilation with a wind velocity exceeding 0.4 m/s in the center of living room. However, its passive cooling effect on indoor space did not improve by increasing the ventilation, due to the inflow of warmer outdoor air. To solve this problem, the necessary optimization of the passive cooling design should be conducted near floor-level windows to cool the introduced airflow.

## 5. Conclusions

- In this study, we proposed a ventilation model that combined a passive cooling design with natural ventilation, using floor-level windows. The passive cooling design consisted of a water retentive block, plants, and dripping pipes placed in front of the floor-level windows. Based on the results of the field experiment and CFD-based simulation, we conclude that the passive cooling design reduced the semi-outdoor and indoor temperatures, and increased the relative humidity.
- The CFD-based simulation model applied in this study was validated by a measurement-to-simulation comparison on a late summer day (air temperature up to 32 °C with a relatively high-speed wind up to around 6 m/s), and was proved to be valid to test the effect of passive cooling design in terms of air temperature, wind velocity, humidity and MRT with acceptable errors.
- With the floor-level windows and skylight open during the ventilation period, a flow path formed inside that inflow, with the flow mainly originating from the western floor-level windows and the skylight, to then escape from the northern floor-level windows.
- Regarding the type of floor-level windows, the side hung type performed better in introducing airflow inside the house; side hung windows with an opening angle of 60° appear to be the best choice, in terms of the increasing of ventilation, since the wind velocity reached 0.4 m/s in the center of the living room. However, the indoor thermal comfort was not improved (SET*s mainly of around 27 °C and 28 °C, above the comfort range) by enhancing the ventilation. To solve this problem, future studies should discuss and explore the configuration of the passive cooling design near floor-level windows.

**Author Contributions:** Conceptualization, B.Q.; data curation, B.Q.; formal analysis, X.X.; resources, T.A.; validation, B.Q.; writing—original draft, B.Q.; writing—review & editing, X.X. and L.Z.; supervision, T.A. All authors have read and agreed to the published version of the manuscript.

**Funding:** This research received no external funding.

**Conflicts of Interest:** The authors declare no conflict of interest.

## References

1. NASA Earth Obeservatory. World of Change: Global Temperatures. 2022. Available online: https://earthobservatory.nasa.gov/world-of-change/global-temperatures (accessed on 20 June 2022).
2. Arakawa, R.; Tsutsumi, J.; Nakamatsu, R. A study on historical change of residential houses and their indoor thermal environment in subtropical Okinawa. *Trans. Archit. Inst. Jpn.* **2007**, *618*, 109–114.
3. International Energy Agency (IEA). *The Future of Cooling: Opportunities for Energy-Efficient Air Conditioning*; International Energy Agency (IEA): Paris, France, 2018.
4. Cook, J. *Passive Cooling*; Arizona State Univ.: Tempe, AZ, USA, 1989.
5. Givoni, B. Performance and applicability of passive and low-energy cooling systems. *Energy Build.* **1991**, *17*, 177–199. [CrossRef]
6. Abro, R.S. Recognition of passive cooling techniques. *Renew. Energy* **1994**, *5*, 1143–1146. [CrossRef]
7. Chen, J.; Brager, G.S.; Augenbroe, G.; Song, X. Impact of outdoor air quality on the natural ventilation usage of commercial buildings in the US. *Appl. Energy* **2019**, *235*, 673–684. [CrossRef]
8. Kamal, M.A. An Overview of Passive Cooling Techniques in Buildings: Design Concepts and Architectural Interventions. *Civ. Eng. Archit.* **2012**, *55*, 84–97.
9. Geros, V.; Santamouris, M.; Tsangrasoulis, A.; Guarracino, G. Experimental evaluation of night ventilation phenomena. *Energy Build.* **1999**, *29*, 141–154. [CrossRef]
10. Chen, J.; Saunders, S.C.; Crow, T.R.; Naiman, R.J.; Brosofske, K.D.; Mroz, G.D.; Brookshire, B.L.; Franklin, J.F. Microclimate in Forest Ecosystem and Landscape Ecology: Variations in local climate can be used to monitor and compare the effects of different management regimes. *Bioscience* **1999**, *49*, 288–297. [CrossRef]
11. Yang, A.S.; Juan, Y.H.; Wen, C.Y.; Chang, C.J. Numerical simulation of cooling effect of vegetation enhancement in a subtropical urban park. *Appl. Energy* **2017**, *192*, 178–200. [CrossRef]
12. Wong, P.P.Y.; Lai, P.C.; Low, C.T.; Chen, S.; Hart, M. The impact of environmental and human factors on urban heat and microclimate variability. *Build. Environ.* **2016**, *95*, 199–208. [CrossRef]
13. Matsumoto, F.; Ichinose, T.; Shiraki, Y.; Lee, L. Climatological study about effect of ventilation by a large restoration of inner-city river—A case of Cheong-Gye Stream in Seoul, South Korea. *Jpn. J. Biometeorol.* **2009**, *46*, 69–80.
14. Del Rio, M.A.; Asawa, T.; Hirayama, Y.; Sato, R.; Ohta, I. Evaluation of passive cooling methods to improve microclimate for natural ventilation of a house during summer. *Build. Environ.* **2019**, *149*, 275–287. [CrossRef]
15. Lee, T.C.; Asawa, T.; Kawai, H.; Sato, R.; Hirayama, Y.; Ohta, I. Multipoint measurement method for air temperature in outdoor spaces and application to microclimate and passive cooling studies for a house. *Build. Environ.* **2017**, *114*, 267–280. [CrossRef]
16. Rouleau, J.; Gosselin, L. Probabilistic window opening model considering occupant behavior diversity: A data-driven case study of Canadian residential buildings. *Energy* **2020**, *195*, 116981. [CrossRef]
17. Toe, D.H.C.; Kubota, T. Comparative assessment of vernacular passive cooling techniques for improving indoor thermal comfort of modern terraced houses in hot–humid climate of Malaysia. *Sol. Energy* **2015**, *114*, 229–258. [CrossRef]
18. Xie, X.; Sahin, O.; Luo, Z.; Yao, R. Impact of neighbourhood-scale climate characteristics on building heating demand and night ventilation cooling potential. *Renew. Energy* **2020**, *150*, 943–956. [CrossRef]
19. Sunaga, N.; Onodera, H.; Kumakura, E.; Ogino, T. Actual state data and methods for improving the indoor thermal environment of apartment houses in the hot–humid regions of Japan. *J. Hous. Res. Found.* **2019**, *45*, 83–94.
20. Horikoshi, T. Basic Principle of a Buffer Zone between Indoor and Outdoor as Environmental Control Devices in Dwelling Houses. *Trans. Soc. Heat. Air Cond. Sanit. Eng. Jpn.* **2017**, 265–268.
21. Yuta, I.; Kengo, K.; Ko, N. The study of the architectural style of tea house by the multivariable analysis using the data of the presence of absence of elements. *J. Archit. Plan.* **2015**, *80*, 2365–2373.
22. Saito, M.; Nasu, S. Luminous Performance of Ji-mado as a Daylighting System In Snowy Region. In Proceedings of the 2005 World Sustainable Building Conference, Tokyo, Japan, 27–29 September 2005; pp. 27–29.
23. Lee, T.C.; Yoon, S.H. A measurement on cold storage of phase change material on the floor of the building with night natural ventilation. *J. Archit. Inst. Korea* **2021**, *37*, 151–156.
24. Jiang, L.; Tang, M. Thermal analysis of extensive green roofs combined with night ventilation for space cooling. *Energy Build.* **2017**, *156*, 238–249. [CrossRef]
25. Lai, D.; Liu, W.; Gan, T.; Liu, K.; Chen, Q. A review of mitigating strategies to improve the thermal environment and thermal comfort in urban outdoor spaces. *Sci. Total Environ.* **2019**, *661*, 337–353. [CrossRef] [PubMed]
26. Seina, U.; Onshi, A.; Masayuki, S. Evaluation and examination of measures toward promoting planting green at detached houses. *J. Jpn. Soc. Civ. Eng. Ser. G* **2016**, *72*, I-109–I-117.

27. Motofumi, M.; Akira, H.; Takashi, A.; Yoshie, I. An experiment on the fundamental performance of an evaporative cooling pavement system during summer:development of an evaporative cooling pavement system and cooling effect simulation model forurban thermal environment Part1. *J. Jpn. Soc. Civ. Eng. Ser. G* **2006**, *71*, 51–58.
28. He, J.; Hoyano, A. Numerical Analysis on the Mitigating Effects of Evaporative Cooling Strategies on the Heat Island Potential for Urban Blocks. *J. Heat Isl. Inst. Int.* **2007**, *2*, 6–13.
29. Mayumi, Y.; Hiroyuki, T.; Koichi, N. Reproducibility of the Atmosphere-Subsurface-Coupled Hydrothermal Environment Model. *J. Heat Isl. Inst. Int.* **2010**, *5*, 24–32.
30. Architectural Institute of Japan. *AIJ Benchmarks for Validation of CFD Simulations Applied to Pedestrian Wind Environment around Buildings Architectural Institute of Japan*; Architectural Institute of Japan: Tokyo, Japan, 2016; ISBN 9784818950016.
31. Porras-Amores, C.; Mazarrón, F.R.; Cañas, I.; Villoría Sáez, P. Natural ventilation analysis in an underground construction: CFD simulation and experimental validation. *Tunn. Undergr. Space Technol.* **2019**, *90*, 162–173. [CrossRef]
32. Xiao, H.; Cinnella, P. Quantification of model uncertainty in RANS simulations: A review. *Prog. Aerosp. Sci.* **2019**, *108*, 1–31. [CrossRef]
33. Ryo, S.; Masanari, U.; Tatsuo, N. Effective Evaluation of Natural Ventilation System. *Trans. Soc. Heat. Air Cond. Sanit. Eng. Jpn.* **2017**, *4*, 1–4.
34. Wang, H.; Chen, Q. Modeling of the impact of different window types on single-sided natural ventilation. *Energy Procedia* **2015**, *78*, 1549–1555. [CrossRef]
35. Heiselberg, P.; Svidt, K.; Nielsen, P.V. Characteristics of airflow from open windows. *Build. Environ.* **2001**, *36*, 859–869. [CrossRef]
36. Liu, T.; Lee, W.L. Using response surface regression method to evaluate the influence of window types on ventilation performance of Hong Kong residential buildings. *Build. Environ.* **2019**, *154*, 167–181. [CrossRef]
37. Zhai, Y.; Wang, Y.; Huang, Y.; Meng, X. A multi-objective optimization methodology for window design considering energy consumption, thermal environment and visual performance. *Renew. Energy* **2019**, *134*, 1190–1199. [CrossRef]
38. Von Grabe, J. Flow resistance for different types of windows in the case of buoyancy ventilation. *Energy Build.* **2013**, *65*, 516–522. [CrossRef]
39. Amaral, A.R.; Rodrigues, E.; Gaspar, A.R.; Gomes, Á. A thermal performance parametric study of window type, orientation, size and shadowing effect. *Sustain. Cities Soc.* **2016**, *26*, 456–465. [CrossRef]
40. Kazuo, F.; Hiroshi, I.; Shigeru, G.; Satoshi, A.; Junji, S. An experiment on SET* and thermal comfort of Japanese. *Trans. Soc. Heat. Air Cond. Sanit. Eng. Jpn.* **1993**, *18*, 139–147.
41. Kenichi, H. Discussion on error of PMV and comfort range under the approximate method between air temperature and MRT. *Trans. Soc. Heat. Air Cond. Sanit. Eng. Jpn.* **2006**, *109*, 29–32.
42. Del Rio, M.A.; Asawa, T.; Hirayama, Y. Modeling and validation of the cool summer microclimate formed by passive cooling elements in a semi-outdoor building space. *Sustainability* **2020**, *12*, 5360. [CrossRef]
43. Liu, J.; Heidarinejad, M.; Pitchurov, G.; Zhang, L.; Srebric, J. An extensive comparison of modified zero-equation, standard k-ε, and LES models in predicting urban airflow. *Sustain. Cities Soc.* **2018**, *40*, 28–43. [CrossRef]
44. Du, Y.; Mak, C.M.; Ai, Z. Modelling of pedestrian level wind environment on a high-quality mesh: A case study for the HKPolyU campus. *Environ. Model. Softw.* **2018**, *103*, 105–119. [CrossRef]
45. McAdams, W.H.; William, H. *Heat Transmission*, 3rd ed.; McGraw-Hill: New York, NY, USA, 1954.
46. Hosoi, F.; Omasa, K. Estimating vertical leaf area density profiles of tree canopies using three-dimensional portable lidar imaging. *Scanning* **2009**, *64*, 151–158.
47. Nemoto, H. *Research on the Passive Cooling Effect on Residential House by Adjustment of Plants on Microclimate and Natural Ventilation*; Tokyo Institute of Technology: Yokohama, Japan, 2014.
48. Kenji, K.; Masamiki, O.; Ken-ichi, N. Wind tunnel experiments on drag coefficient of trees with the leaf area density as a reference area. *J. Environ. Eng.* **2004**, *578*, 71–77.
49. Asawa, T.; Fujiwara, K.; Hoyano, A.; Shimizu, K. Convective heat transfer coefficient of crown of Zelkova Serrata. *J. Environ. Eng.* **2016**, *81*, 235–245. [CrossRef]
50. Kiyono, T.; Asawa, T.; Hoyano, A.; Shimizu, K. Weighing whole tree transpiration rate of urban trees and analysis of trees Morpho-Physiological effects. *J. Environ. Eng.* **2015**, *80*, 599–608. [CrossRef]
51. SIMTEQ Engineering (Pty) Ltd. Tutorials of Cradle CFD 2020-csSTREAM. Available online: https://simteq.co.za/blog/cradle-getting-started/ (accessed on 20 June 2022).
52. Tetens, O. Uber einige meteorologische Begriffe. *Z. Geophys.* **1930**, *6*, 297–309.